Revealing the Design Principles of High-Performance Biological Composites Using Ab initio and Multiscale Simulations: The Example of Lobster Cuticle

By *Svetoslav Nikolov, Michal Petrov, Liverios Lymperakis, Martin Friák, Christoph Sachs, Helge-Otto Fabritius, Dierk Raabe,* * and *Jörg Neugebauer*

In the course of evolution nature developed materials based on organic–inorganic nanocomposites with complex, hierarchical organization from Ångstroms to millimeters tailored via molecular self-assembly.[1–3] Such materials possess outstanding stiffness, toughness, and strength related to their low density, while the mechanical characteristics of their underlying constituents are rather modest.[2,4] This remarkable performance is a consequence of their hierarchical structure, the specific design at each level of organization, and the inherent strong heterogeneity[4] resulting in the accommodation of macroscopic loadings by different deformation mechanisms at different length scales. Therefore, to understand the macroscopic mechanical properties of the tissue, one should take into account its structure–property relations at all length scales down to the molecular level.

To date, this key challenge has been only partly addressed due to severe obstacles in obtaining mechanical and structural data at the nanometer scale. The mechanical properties of important proteins and biominerals as well as some details about their exact structure are still unknown. A powerful tool to overcome these difficulties and to better understand the structure–property relationships in biomaterials is multiscale modeling encompassing all length scales.[3,5] Some progress in the development of multiscale structure–property relationships for mineralized tissues has been achieved by combined modeling and experimental approaches applied to bone,[4] nacre,[6] and fish skin armor.[7] However, these approaches do not explicitly integrate a molecular-level description and use continuum mechanics at the meso- and macroscale (e.g., finite element analysis) coupled with experimental data obtained, for example, by nanoindentation. A

[*] Prof. D. Raabe, Dr. M. Petrov, Dr. L. Lymperakis, Dr. M. Friák,
    Dr. H. Fabritius, Prof. J. Neugebauer
    Max-Planck-Institut für Eisenforschung
    Max-Planck Str. 1, 40237 Düsseldorf (Germany)
    E-mail: d.raabe@mpie.de
    Prof. S. Nikolov
    Institute of Mechanics, Bulgarian Academy of Sciences
    Acad. G. Bonchev Str. Bl. 4 1113 Sofia (Bulgaria)
    E-mail: sv.nikolov@imbm.bas.bg
    Dr. C. Sachs
    Department of Materials Science and Engineering
    MIT, 77 Massachusetts Ave, Cambridge, MA 02139-4307 (USA)
    E-mail: csachs@mit.edu

more advanced multiscale modeling has been proposed for collagen-based biomaterials,[3,5] where molecular-dynamics calculations are applied to individual tropocollagen molecules,[8] while the deformation behavior of single collagen fibrils[9] at the mesoscale and of soft collagen tissues[10] at the macroscale has been modeled by adopting continuum-mechanical concepts.

First-principles calculations, based on quantum mechanics and density functional theory (DFT), that are free of adjustable or experimental parameters have recently evolved as a versatile and accurate tool to study fundamental biological mechanisms and structures on the atomic scale. However, due to the complexity and the hierarchical nature of biomaterials, the application of these techniques is still out of reach to study macroscopic mechanical behavior. We therefore propose a new approach combining ab initio calculations with hierarchical homogenization that allows us to study structure–property relations including all length scales.

To describe the key concepts of this approach and to demonstrate its applicability we choose a tissue containing chitin, the second most abundant natural polymer on earth after cellulose. Chitin-based composites serve as exoskeleton material for more than 90% of all animal species, a fact that demonstrates their extremely adaptive potential to realize a vast range of natural materials. In this Communication, the cuticle of a large crustacean, the lobster *Homarus americanus*, is discussed as a model material. The crustacean cuticle is one of the oldest natural materials for structural and armor applications. Crustacea, such as crab, lobster, crayfish, or shrimp, are already present in the fossil record of the Early Cambrian period (~515 Myr ago) and, thus, among the most successful animals living on earth.[11] One of the reasons for the versatility of crustaceans is their functional body design, featuring a hard, chitin-based mineralized exoskeleton. Another consideration for choosing the cuticle of *H. americanus* is that extensive experimental data are available on its microstructure and crystallographic texture.[12–19] These data are required as an input to construct the multiscale approach, while the experimentally measured mechanical properties of the cuticle[14–17] allow to quantitatively validate the accuracy of our model.

The cuticle consists of chitin in the form of crystalline nanofibrils,[20,21] various proteins, mineral nanoparticles (mostly amorphous calcium carbonate (ACC) but also some crystalline calcite),[18] and water. A schematic representation of the hierarchical organization of the cuticle is shown in Figure 1. It illustrates several generic design principles of crustacean
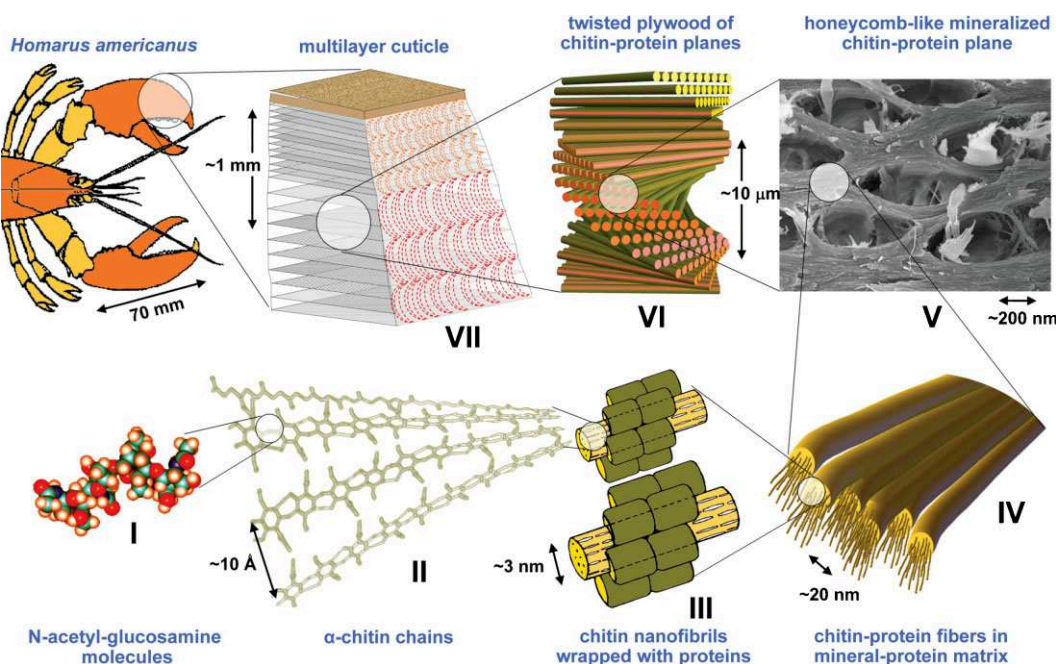
Figure 1. Hierarchical structure of the lobster cuticle: I) *N*-acetyl-glucosamine molecules,[24] II) antiparallel chains of α-chitin,[24] III) chitin–protein nanofibrils,[20] IV) chitin–protein fibers in a mineral–protein matrix[21] (not shown), V) cuticle with pore canal system[17] (in-plane cross-section), VI) twisted plywood structure[22], and VII) three-layered cuticle.[14]

exoskeletons, namely: i) reinforcement achieved by chitin–protein fibers[20,21] organized in a twisted plywood (Bouligand) structure resembling a cholesteric liquid crystal[22] (Fig. 1VI), ii) a mineral–protein matrix accommodating and stiffening the chitin network, iii) multilayer design at the macroscopic level (Fig. 1VII),[23] and iv) strong heterogeneity at the nanometer scale between soft proteins and stiff minerals (or chitin fibrils). In addition, the lobster cuticle exhibits a well-developed, honeycomb-like system of pore canals[12] (Fig. 1V), which facilitates biomineralization by water-mediated transport of calcium and other ions across the cuticle, provides for fast cuticle growth during the molting cycle, and reduces its density.

In Figure 1, at the lowest level of hierarchy, *N*-acetyl-glucosamine molecules (I) build polymer chains of α-chitin (II);[24] 19–25 chains arrange anti-parallel in long crystalline α-chitin nanofibrils.[20,21] These nanofibrils are individually wrapped with proteins (III)[20] and clusters to form chitin–protein fibers embedded in a mineral–protein matrix (IV). In the plane of the cuticle, the mineralized tissue appears as a honeycomb-like structure with elliptic openings (V).[12,13] At the next higher hierarchy level, the chitin–protein planes gradually rotate around the normal direction of the cuticle, which results in a twisted plywood (VI)[22] pierced by canals in the form of helicoidal ribbons with an elliptical cross-section. At the macroscopic scale (VII), the cuticle consists of three layers:[23] a thin, waxy epicuticle, an exocuticle (thickness ~200–300 μm), and an endocuticle (thickness ~250 μm–2.5 mm).[16] The exocuticle can be viewed as a harder and stiffer endocuticle with higher mineral content, smaller canal pores, and a smaller pitch of rotation of the twisted plywood (~10 μm) compared to that of the endocuticle (~30 μm).[14] Interestingly, such a multilayer

design with a harder outer layer is also found in other "armored" species, e.g., the bony skin of the fish *Polypterus senegalus*,[7] and is apparently well adapted to resist concentrated compressive loads produced, for example, by predator biting.

Due to the above-outlined complex structure, the modeling of the mechanical properties is challenging. Therefore, we have developed a hierarchical constitutive model (Fig. 2), which includes ab initio calculations at the nanometer scale where experimental data are missing and mean-field homogenization for higher hierarchy levels.

For a given hierarchy level, we define a representative volume element (RVE) of the heterogeneous material and find its homogenized properties using an appropriate micromechanical model. These properties are then used to inform the modeling of the microstructure at the next higher level. The procedure is repeated in a bottom-up order to cover all observed microstructures at all length scales from 10^{-9} to 10^{-3} m. The approach described in the following is general and can be applied to other biocomposites.

The multiscale approach starts at the atomic scale where the electronic structure determines the interatomic bonding and eventually the elastic properties of the material (Fig. 2I,II). Because of the difficulty to isolate and test single α-chitin nanofibrils, so far, it has not been possible to experimentally measure their 3D elastic constants. To establish the positions of the hydrogen atoms and the hydrogen bonds in α-chitin, which are not accessible by X-ray crystallography,[24] a hierarchical computational approach is employed, which combines valence force field molecular dynamics (VFFMD) with tight binding (TB) and DFT calculations. In a first step, VFFMD simulations were used within the framework of a probabilistic conformational
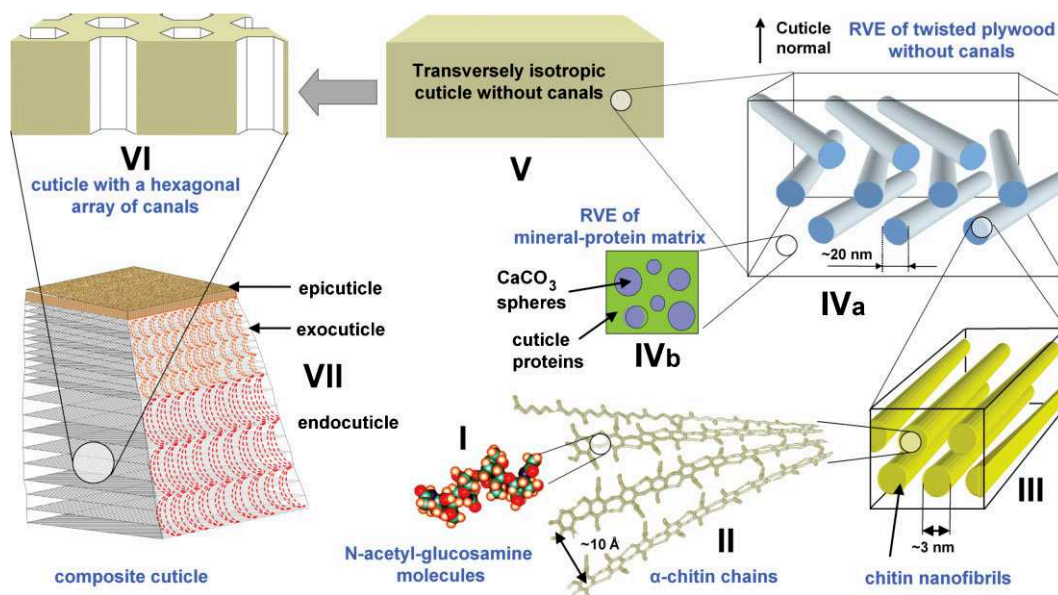
Figure 2. Hierarchical modeling of the lobster cuticle: I,II) α-chitin properties via ab initio calculations. III) Representative volume element (RVE) for a single chitin–protein fiber. IVa) RVE for chitin–protein fibers arranged in twisted plywood and embedded in mineral–protein matrix. IVb) RVE for the mineral–protein matrix. V) Homogenized twisted plywood without canals. (I) Homogenized plywood pierced with hexagonal array of canals. VII) Three-layered cuticle.

search, which resulted in a representative set of conformations.[25] Starting from a rather arbitrary atomic geometry that conserves the chemical formula of α-chitin, an extended room-temperature molecular dynamic (MD) run sampled the multidimensional Born–Oppenheimer surface.[26] Based on the criteria of (i) minimum potential energy and (ii) maximum number of hydrogen bonds, approximately 10^2 out of 10^5 structures emerged as likely from our probabilistic conformational search. Subsequently, the properties of the thus chosen configurations have been refined and re-checked employing self-consistent DFTB (density-functional-based tight binding calculations).[27] Due to the high structural flexibility of crystalline α-chitin, the calculated points do not follow a smooth curve and show a rather scattered behavior. This problem is overcome by using an adiabatic/quasistatic approach: each calculated point is derived from the previously relaxed atomic geometry by applying a small deformation. About 10 low-energy structures emerged from the TB calculations and have been used as input to the subsequent parameter-free calculations performed within DFT[28,29] using pseudopotentials and planewaves.[30,31] The resulting lattice constants are for an orthorhombic unit cell ($a = 4.98$ Å, $b = 19.32$ Å, $c = 10.45$ Å) and agree within 5% with the experimentally measured cell parameters[24] ($a = 4.74$ Å, $b = 18.86$ Å, $c = 10.32$ Å). The obtained ground-state structure of α-chitin as well as the response of the biocrystal to uniaxial small deformations applied along the unit-cell vectors a, b, and c are shown in Figure 3.

The corresponding stiffness tensor obtained with DFT calculations for orthorhombic crystals is expressed in Equation (1).[32]

$$\underline{C_{CH}}\,(\text{GPa}) = \begin{bmatrix} 119 & 0.1 & 1.1 & 0 & 0 & 0 \\ 0.1 & 28 & 2 & 0 & 0 & 0 \\ 1.1 & 2 & 24 & 0 & 0 & 0 \\ 0 & 0 & 0 & 5 & 0 & 0 \\ 0 & 0 & 0 & 0 & 8 & 0 \\ 0 & 0 & 0 & 0 & 0 & 2 \end{bmatrix} \quad (1)$$

The tensor is defined in a local Cartesian coordinate frame where the vectors of the orthorhombic unit of α-chitin a, b, and c (chain direction) are along the axes 2, 3, and 1, respectively.
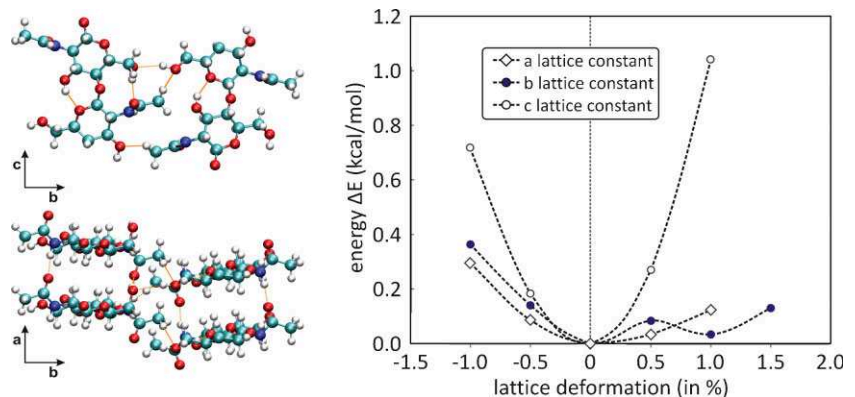

Figure 3. Left: Theoretically determined structure of single-crystalline α-chitin: a, b, and c (chain direction) denote the unit-cell vectors. The spheres (atoms) are colored as follows: red—O, blue—N, turquoise—C, white—H; the orange lines represent H-bonds. Right: total unit-cell energy versus uniaxial strain profiles for deformations along a, b, and c. Positive (negative) values along the x-axis denote tensile (compressive) strain, respectively.

COMMUNICATION

Based on the elastic tensor, it is evident that α-chitin is much stiffer in the chain direction c compared to the transverse directions. This is due to strong covalent bonds, which dominate along the chain axis, compared to the rather weak H-bonds, which are responsible for cohesion in the transverse directions.

The effective properties at higher hierarchy levels are calculated using homogenization methods[33–35] adapted to the specific microstructure. We consider only the elastic properties of intact cuticle at small strains. For the input, the properties of each phase within the composite as well as the volume fractions, the shapes, and the orientations of each of the dispersed phases are considered. When necessary, three-point estimates are used where, in addition to the above-mentioned parameters, the specific arrangement of the dispersed phases is taken into account via statistical correlation functions.[36] The unknown properties of the cuticle proteins are identified from experimental data for a wet tissue in order to investigate the material in a state close to that in the living animal. Experimentally, Young's modulus of a dry cuticle is about 10–15% higher in the normal direction and roughly 25–50% higher in the in-plane direction, compared to that of a hydrated cuticle.[16,17] The difference between wet and dry tissue is even more pronounced during damage and failure but we do not consider these issues here. In our analysis, the presence of water is implicitly taken into account in the identification of the protein properties. In a first approximation, perfect bonding without slippage is assumed at the interfaces. The mineral–protein matrix (Fig. 2IVb) is assumed to consist of calcium carbonate spherules embedded in proteins because biogenic ACC in lobster, stabilized by macromolecules and small amounts of Mg and phosphate,[37] always grows spherically.[38]

The RVE of a single chitin–protein fiber (Fig. 2III) is modeled as a long-fiber composite with an isotropic soft protein matrix and aligned α-chitin cylindrical fibers. The homogenized elastic behavior is obtained with a classical Mori–Tanaka scheme.[33] This model provides very reasonable predictions for the overall properties of two phase composites consisting of aligned inclusions or spheres, as long as the volume fraction of the dispersed phase is equal or less than 0.2,[36] which is the case here. Young's modulus and Poisson's ratio of the proteins within a single chitin–protein fiber are identified as 4 MPa and 0.49, respectively. These values have been deduced from tensile experiments on wet membrane samples, which contain chitin but not minerals.[16] The Bouligand plywood structure with a system of pore canals (Fig. 1V,VI) is modeled in two steps. First, the effective (transversely isotropic) properties of the bulk plywood composite without canals are found. Then, the pore canal system is taken into account and the cuticle is approximated as a honeycomb with thick walls. The RVE of the bulk cuticle (Fig. 2IVa) is modeled as plywood where each ply consists of a mineralized isotropic matrix reinforced with aligned chitin–protein fibers. The neighboring plies are rotated at a constant fixed angle with respect to each other. The homogenized properties of each ply are found using a Mori–Tanaka scheme.[33] For the effective properties of the twisted plywood, a Voigt estimate is used.

The mineral–protein matrix in the bulk tissue (Fig. 2IVb) is modeled via Torquato's three-point approximation,[34] which has been proven to be the best estimate for two-phase isotropic composites with high volume fraction of the inclusions.[39] In our case, the volume fraction of the $CaCO_3$ spherules in the mineral–protein matrix can be as high as 0.76 in the endocuticle and even higher in the exocuticle.[16] The properties of biological ACC are not known exactly and are assumed to be equal to those of synthetic ACC spherules, for which the experimentally measured Young modulus and Poisson ratio have been reported to be 37 GPa and 0.35, respectively.[40] The unknown properties of the proteins in the mineral–protein matrix (Fig. 2IVb) have been fixed after tuning the model predictions to the experimental data, with Young's modulus and Poisson's ratio identified as 1.0 GPa and 0.46, respectively. The in-plane properties of the cuticle with a canal pore system (Fig. 2 VI) are found using a three-point Torquato estimate for 2D regular honeycombs with thick walls.[35] The in-plane area fraction of the canals has an average value of ∼0.3, which was calculated from scanning electron microscopy (SEM) images and from scanning Raman spectroscopy. The out-of-plane properties of the cuticle are estimated using a Voigt average over Young's moduli and Poisson's ratios of the bulk cuticle and the holes in the normal direction, which provides good accuracy along the hole axis.[41]

The samples used for the mechanical tests[16] were dissected from the claws of a large adult, nonmolting American lobster. The outer waxy layer and the exocuticle were removed by machining. The elastic moduli and Poisson ratios of the cuticle were obtained by performing compression and tensile tests in the normal and the in-plane directions. The grade of mineralization was determined using thermogravimetric analysis. A total of 24 tensile-test specimens were prepared to perform loading tests in the in-plane direction of the cuticle. A set of 16 compression-test specimens was prepared for testing the cuticle in its normal direction. The samples were kept in their natural wet state. The tests were performed on a miniaturized test rack combined with digital image correlation (DIC) to acquire strain data.[15,42] DIC recognizes the geometrical changes in the gray-scale distribution of surface patterns before and after straining.[15,42] The input pattern was created by spraying graphite aerosol on the white cuticle surfaces. The loading strain rate was $0.001\,s^{-1}$.

Since the size distribution and the arrangement of the ACC spherules in lobster cuticle are not known, we used our hierarchical approach to test three different hypotheses for the microstructure of the mineral–protein matrix (Fig. 2IVb), namely: i) overlapping spheres, ii) a random array of impenetrable spheres with polydispersity in size, and iii) symmetric cell material[43] of spheres with varying diameters. The latter has been proposed as a purely theoretical concept 40 years ago and is defined by the following procedure.[43] First, space is divided into spherical cells with different diameters so that their sizes are distributed in a statistically homogeneous and isotropic manner throughout the material. Then, the property of the mineral (with probability ϕ) or protein (with probability $1-\phi$) is assigned to each cell randomly and independently from the properties of the other cells, so that the volume fraction ϕ of the spheres has the property of the mineral and the volume fraction $1-\phi$ has the property of the protein. The resulting composite is macroscopically homogeneous and isotropic.

In Figure 4 the predicted Young moduli and Poisson ratios are compared with data obtained by tension and compression tests on
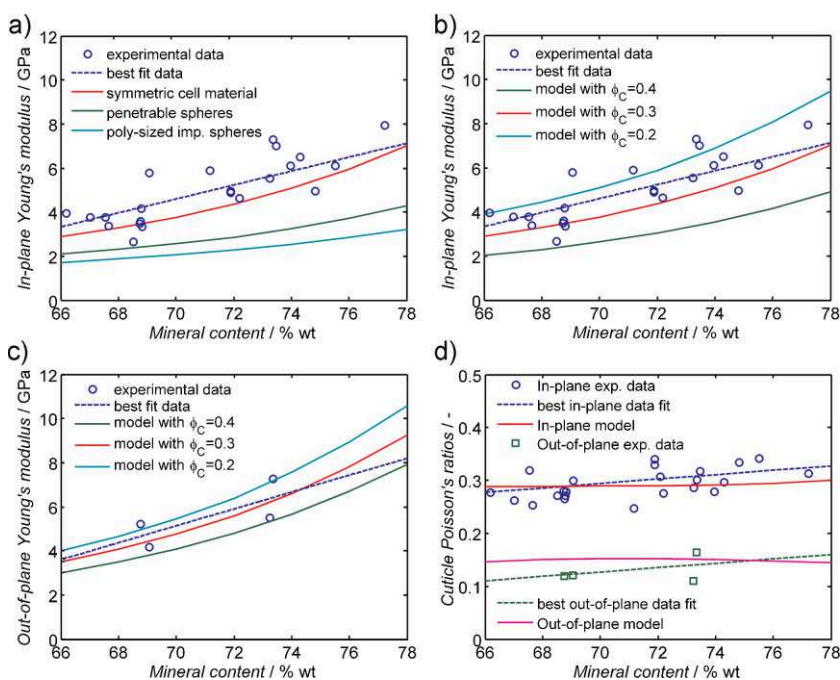
Figure 4. a) In-plane Young modulus as a function of the mineral–protein matrix microstructure and the mineral content for $\phi_C = 0.3$. b) In-plane modulus for different canal-pores area fractions versus mineral content. c) Out-of-plane Young modulus for different canal-pores area fractions versus mineral content. Symbols: experimental data,[14] lines: model predictions. d) Cuticle in-plane and out-of-plane Poisson ratios versus mineral content.

hydrated endocuticle samples.[16] To calculate the effective elastic properties, the experimentally obtained mineral weight fractions (66–78 wt%, measured by thermogravimetric analysis[16]) are converted to volume fractions (∼0.59–0.76 for a volume fraction of the chitin–protein fibers of 0.2) and used as a model parameter. Figure 4a shows the predicted and the measured in-plane Young modulus data of the cuticle as a function of the mineral content and of the above-mentioned three possible microstructures of the calcium carbonate spherules in the mineral–protein matrix. The area fraction of the canals, ϕ_C, is set to 0.3, in accordance with the average experimentally measured values.

Figure 4a clearly shows that the only mineral–protein microstructure that can explain the strong increase of Young's modulus (from ∼3 to ∼8 GPa) with increasing mineral content is that of a symmetric cell material of $CaCO_3$ spherules embedded in a protein matrix. For a typical area pore fraction of 0.3, the model underestimates the best data fit with a maximum error of 20% for a mineral content of 70 wt% using the symmetric cell material arrangement, while the assumptions of penetrable spheres or of a random array of polydisperse spheres underestimate the in-plane modulus by a factor of 2. This is a remarkable result. To the best of our knowledge, symmetric cell materials have not been realized synthetically. Until now, they have only been a purely theoretical design concept, which maximizes stiffness for a given volume fraction of the constituents. In fact, this concept has been introduced by Miller[43] in order to construct more realistic upper (lower) bounds for the effective properties of two-phase composites compared to the Hashin–Shtrikman bounds[44] (the best possible bounds in terms of volume fraction alone). Thus, a symmetric cell

material possesses the highest possible stiffness among all two-phase composites with hard spherical inclusions except for the Hashin–Shtrikman assembly of densely packed polydisperse-coated spheres.[44] It seems that the biomineralization kinetics in lobster, and probably in other species, indeed employs this highly optimized symmetric cell material concept.

In Figure 4b the in-plane Young modulus of the cuticle is plotted against the mineral content for different area fractions of the pore canals ranging from 0.2 to 0.4, which cover all of the experimentally measured values. It can be seen that most of the scattering in the measured modulus can be explained by the biological variation of the in-plane area fraction of the cuticle canals and the variable mineral content. In Figure 4c, a similar plot for the cuticle out-of-plane Young modulus is shown. Along its normal direction, the cuticle elastic modulus increases with the mineral content similarly to the in-plane modulus. It is higher compared to the in-plane modulus for all studied mineral grades and also less sensitive to the in-plane area fraction of the canals. Figure 4d shows that the experimentally measured Poisson ratios of the cuticle slightly increase with increasing mineral content, while in the model predictions Poisson's ratios remain virtually unchanged. The in-plane Poisson ratio is about 0.3, while along the cuticle normal it is roughly 0.13 for all mineral grades. Our model predicts constant in-plane and out-of-plane Poisson ratios of 0.29 and 0.15, respectively. From the obtained results, we conclude that the multiscale approach is able to successfully reproduce all experimental values and trends. Our results underestimate the experimental in-plane Young modulus by no more than 20%. On the other hand, the out-of-plane elastic modulus and the in-plane Poisson ratio are predicted fairly well with the same set of parameters, while the out-of-plane Poisson ratio is somewhat overestimated by the model. Hence, the results give satisfactory quantitative predictions given the number of approximations and simplifications made in the multiscale model. Our predictions can probably be further improved by using a more realistic representation of the helicoidal pore canals with elliptic cross-sections, e.g., via direct finite-element modeling at a macroscopic length scale. In the present work, the canals are modeled as hexagonal holes with straight walls, which is a somewhat crude but useful approximation. The model does not contain any adjustable parameters but only parameters that are, in principle, experimentally measurable and that are directly related to the structure and the properties of the cuticle constituents. Further validation of the approach requires more reliable data for some unknown properties, for example, those of the cuticle proteins.

Having established the reliability of our theoretical approach, we are now able to analyze how the mechanical properties evolve at various hierarchical levels when moving from the atomic to the macroscopic scale. 3D maps of Young's modulus for selected
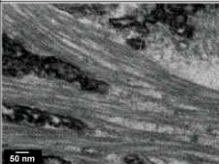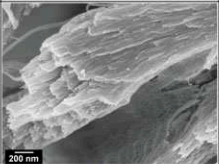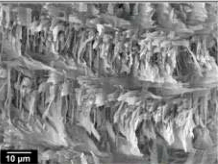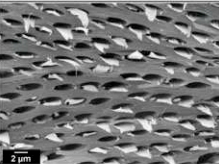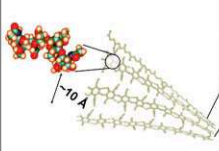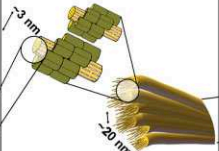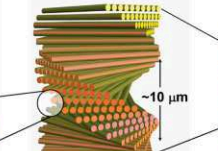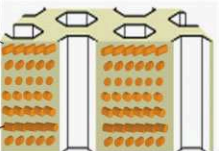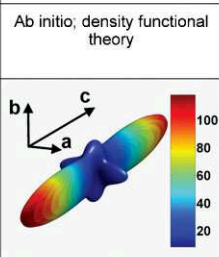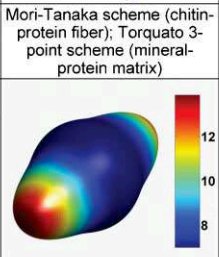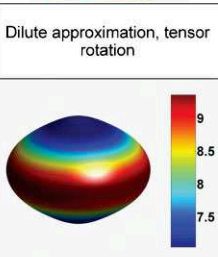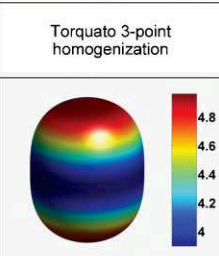
Scale	0.1 nm – 10 nm	10 nm – 100 nm	100 nm – 10 μm	10 μm – 1 mm
Hierarchical structure unit	α-chitin (H-bonded anti-parallel N-acetyl-glucosamine molecular chains)	Mineralized chitin-protein nanofibrils in a planar array	Twisted plywood stack of mineralized chitin-protein planes without pore canals	Twisted plywood stack of mineralized chitin-protein planes with pore canals
Experimental method	Transmission electron microscope	Field emission scanning electron microscope	Field emission scanning electron microscope	Field emission scanning electron microscope
Microstructure				
Schematic				
Simulation method	Ab initio; density functional theory	Mori-Tanaka scheme (chitin-protein fiber); Torquato 3-point scheme (mineral-protein matrix)	Dilute approximation, tensor rotation	Torquato 3-point homogenization
Elastic behavior, 3D maps of Young's modulus [GPa] a,b-axes: basal directions of the chitin unit cell c-axis: longitudinal (chain) axis of the chitin molecule				

Figure 5. Overview of key cuticle microstructures at different length scales including the methods used and the predicted anisotropy for a typical mineral content of 70 wt%.

cuticle hierarchies are given in Figure 5, which provide direct insight into the purpose of the various structures. A surprising outcome of our study is the high anisotropy at the most fundamental level: The modulus along the axial direction of a single-crystalline chitin nanofibril is ~119 GPa, while the modulus in the transverse direction is only 28 GPa. A general trend observed when moving from one hierarchical level to the next is that the overall cuticle anisotropy decreases monotonously. When moving from nanometer- to macroscale the anisotropy ratio changes from 4.25 (single-crystalline chitin), to 1.75 (mineralized chitin–protein nanofibrils), and down to 1.4 (1.25) for the twisted plywood structure without (with) pore canals. The efficient reduction in anisotropy is achieved by several strategies: At the smallest scale by wrapping the needle-like chitin crystallites with soft proteins and, then, embedding the chitin–protein fibers in the isotropic mineral–protein matrix, which also increases significantly the cuticle stiffness along its normal direction. At higher scales by twisting the fibrillar planes and introducing the pore structure.

Our calculations also provide an insight into how nature balances competing properties. On one side, pore canals are vital for the lobster because of its role in biomineralization, while at the same time they weaken the structure. The formation of regular honeycombs with thick walls (i.e., with in-plane area fraction of the pores $\phi_C \leq 0.3$) guarantees the largest possible in-plane stiffness compared to other planar microstructures with the same porosity fraction.[35] This specific geometry ensures that the canal-pore-area fraction is just as large as to simultaneously

ensure optimal cuticle stiffness and maximum fluid transport capacity for fast mineralization. An important issue is how errors and uncertainty at lower hierarchical levels propagate across the length scales and influence the macroscopic behavior. In a preliminary study to address this problem, we performed numerical simulations, where the three largest elastic constants of α-chitin at the lowest hierarchy level were deviated, one at a time, from their values given in Equation (1) by ±20%.

These simulations showed that errors of such magnitude in the α-chitin elastic constants have a negligible effect on the macroscopic behavior due to (i) the very soft proteins wrapping the chitin nanocrystallites and (ii) the cholesteric plywood arrangement. In principle, the model can be extended to finite strains and inelastic behavior but this involves a much more complicated multiscale viscoelastic and elasto-viscoplastic reformulation and numerical implementation and, possibly, a reduced accuracy compared to the small-strain elastic approach. Large-strain inelastic multiscale models for hierarchical materials have been recently proposed (e.g., in the work of Vernerey et al.)[45] but have not yet been applied to hierarchical structures with a degree of complexity close to that of real biomaterials. Besides the restriction to linear elasticity and small strains, our approach has further limitations, most of which are inherent to the homogenization methods as such. For example, while bottom-up multiscale models based on homogenization are efficient and accurate in the prediction of averaged quantities, such as effective stiffness, their predictive capacity decreases significantly when limited regions with high stress and strain gradients as well as

localization phenomena (e.g., localized shear and damage at interfaces) within the representative volume are considered.[46]

In conclusion, we introduced a hierarchical multiscale modeling approach that seamlessly connects the atomic with the macroscopic scale and fully accounts for the hierarchical complexity of biological nanocomposites. At the nanoscale, this methodology allows us to determine mechanical properties and structures that were hitherto not accessible and to follow their fascinating evolution up to the macroscale. An important piece of information that could be deduced from these simulations is the relation between structure and optimum mechanical properties. In the present case we can show that the cholesteric plywood superstructure guarantees that the chitin–protein fibers reinforce the cuticle, provides for transverse isotropy that is well suited to resist macroscopic loads, prevents the propagation of micro-cracks, and is able to dissipate significant amounts of energy during impact loadings. Besides the twisted plywood architecture, the monotonously decreasing anisotropy from lower to higher hierarchy levels illustrates a rather general principle in the biomaterials design, namely that the shortcomings in the properties of biomaterials at lower hierarchical levels are corrected with suitable superstructures at higher levels.

Our approach also allowed for the identification of the dominant factors determining the cuticle stiffness next to the chitin network: i) the mineral content, ii) the specific microstructure of the mineral–protein matrix, and iii) the in-plane area fraction of the pore canals. Another interesting consequence of our analysis is that the hierarchical structure of the lobster cuticle produces – for a given volume fraction of minerals – the stiffest possible armor design,[47] which, at the same time, ensures optimum biomineralization kinetics. The proposed multiscale scheme is not restricted to the chitin-based exocuticle of *H. americanus* but can be applied to other biological nanocomposites provided that their hierarchical microstructure is known in sufficient detail.

Finally, our investigation provides some ideas for the elaboration of high-performance and/or multifunctional composites for shell and plate applications at both a larger scale and the nanometer scale. For example, twisted plywood composites, where each layer is reinforced with high-modulus fibers coated with very soft polymer, could be used for structural and armor applications. Another interesting challenge would be the synthesis of organic–inorganic nanocomposite materials with microstructures close to that of a symmetric cell material. Such materials would possess remarkable, for example, mechanical properties but their fabrication or synthesis would require sophisticated molecular engineering to insure, for example, strong bonding at the interfaces and controlled growth and morphology of the inorganic phase. Despite the recent progress in the de novo synthesis of bioinspired materials,[48] we are still in the beginning of a long journey towards real understanding of the design principles of biomaterials and this makes the creation of viable synthetic analogues even more challenging.

Acknowledgements

[1] P. Fratzl, R. Weinkamer, *Prog. Mater. Sci.* **2007**, *52*, 1263.
[2] M. A. Meyers, P. Y. Chen, A. Y. M. Lin, Y. Seki, *Prog. Mater. Sci.* **2008**, *53*, 1.
[3] M. J. Buehler, S. Keten, T. Ackbarow, *Prog. Mater. Sci.* **2008**, *53*, 1101.
[4] K. Tai, M. Dao, S. Suresh, A. Palazoglu, C. Ortiz, *Nat. Mater.* **2007**, *6*, 454.
[5] M. J. Buehler, Y. C. Yung, *Nat. Mater.* **2009**, *8*, 175.
[6] B. J. F. Bruet, H. J. Qi, M. C. Boyce, R. Panas, K. Tai, L. Frick, C. Ortiz, *J. Mater. Res.* **2005**, *20*, 2400.
[7] B. J. F. Bruet, J. Song, M. C. Boyce, C. Ortiz, *Nat. Mater.* **2008**, *7*, 748.
[8] M. J. Buehler, S. Y. Wong, *Biophys. J.* **2007**, *93*, 37.
[9] M. J. Buehler, *Proc. Natl. Acad. Sci. USA* **2006**, *103*, 12285.
[10] M. J. Buehler, B. Moran, *Ann. Biomed. Eng.* **2009**, *37*, 1117.
[11] T. H. P. Harvey, N. G. Butterfield, *Nature* **2008**, *452*, 868.
[12] D. Raabe, P. Romano, C. Sachs, A. Al-Sawalmih, H.-G. Brokmeier, S.-B. Yi, G. Servos, H. G. Hartwig, *J. Cryst. Growth* **2005**, *283*, 1.
[13] P. Romano, H. Fabritius, D. Raabe, *Acta Biomater.* **2007**, *3*, 301.
[14] C. Sachs, H. Fabritius, D. Raabe, *J. Mater. Res.* **2006**, *21*, 1987.
[15] C. Sachs, H. Fabritius, D. Raabe, *J. Struct. Biol.* **2008**, *161*, 120.
[16] C. Sachs, *Ph.D. Thesis* RWTH Aachen, Germany **2008**.
[17] H.-O. Fabritius, C. Sachs, P. Romano, D. Raabe, *Adv. Mater.* **2009**, *21*, 391.
[18] A. Al-Sawalmih, C. Li, S. Siegel, H. Fabritius, S.-B. Yi, D. Raabe, P. Fratzl, O. Paris, *Adv. Funct. Mater.* **2008**, *18*, 3307.
[19] A. Al-Sawalmih, C. Li, S. Siegel, P. Fratzl, O. Paris, *Adv. Mater.* **2009**, *21*, 1.
[20] J. Blackwell, M. A. Weih, *J. Mol. Biol.* **1980**, *137*, 49.
[21] M.-M. Giraud-Guille, H. Chanzy, R. Vuong, *J. Struct. Biol.* **1990**, *103*, 232.
[22] Y. Bouligand, *Tissue Cell* **1972**, *4*, 189.
[23] N. F. Hadley, *Sci. Am.* **1986**, *255*, 98.
[24] R. Minke, J. Blackwell, *J. Mol. Biol.* **1978**, *120*, 167.
[25] A. K. Rappe, C. J. Casewit, K. S. Colwell, W. A. Goddard, W. M. Skiff, UFF (Universal Force Field), *J. Am. Chem. Soc.* **1992**, *114*, 10024.
[26] http://accelrys.com/products/materials-studio/modules/forcite.html. (last accessed August 2009).
[27] M. Elstner, *Theor. Chem. Acc.* **2006**, *116*, 316.
[28] P. Hohenberg, W. Kohn, *Phys. Rev.* **1964**, *136*, B864.
[29] W. Kohn, L. J. Sham, *Phys. Rev.* **1965**, *140*, A1133.
[30] G. Kresse, J. Furthmueller, *Phys. Rev. B* **1996**, *54*, 11169.
[31] P. E. Blöchl, *Phys. Rev. B* **1994**, *50*, 17953.
[32] P. Ravindran, L. Fast, A. P. Korzhavyi, B. Johansson, *J. Appl. Phys.* **1998**, *84*, 4891.
[33] Y. Benveniste, *Mech. Mater.* **1987**, *6*, 147.
[34] S. Torquato, *J. Mech. Phys. Solids* **1998**, *35*, 1411.
[35] S. Hyun, S. Torquato, *J. Mater. Res.* **2000**, *15*, 1985.
[36] S. Torquato, *Random Heterogeneous Materials: Microstructure and Macro-scopic Properties*, Springer, New York **2002**.
[37] Y. Levi-Kalisman, S. Raz, S. Weiner, L. Addadi, I. Sagi, *Adv. Funct. Mater.* **2002**, *12*, 43.
[38] A. Shechter, A. Berman, A. Singer, A. Freiman, M. Grinstein, J. Erez, E. D. Aflalo, A. Sagi, *Biol. Bull.* **2008**, *214*, 122.
[39] J. Segurado, J. Llorca, *J. Mech. Phys. Solids* **2002**, *50*, 2107.
[40] M. Faatz, W. Cheng, G. Wegner, *Langmuir* **2005**, *21*, 6666.

[41] I. V. Andrianov, V. V. Danishevs'kyy, D. Weichert, *Eur. J. Mech. A* **2002**, *21*, 1019.

[42] C. Sachs, H. Fabritius, D. Raabe, *J. Struct. Biol.* **2006**, *155*, 409.

[43] M. N. Miller, *J. Math. Phys.* **1969**, *10*, 1988.

[44] Z. Hashin, S. Shtrikman, *J. Appl. Phys.* **1962**, *33*, 3125.

[45] F. Vernerey, W. K. Liu, B. Moran, *J. Mech. Phys. Solids* **2007**, *55*, 2603.

[46] S. Ghosh, in *Multiscale Modeling and Simulation of Composite Materials and Structures*, (Eds: Y. W. Kwon, D. H. Allen, R. Talreja), Springer, New York **2007**, Ch. 3.

[47] D. Raabe, C. Sachs, P. Romano, *Acta Mater.* **2005**, *53*, 4281.

[48] H. D. Espinosa, J. E. Rima, F. Barthelat, M. J. Buehler, *Prog. Mater. Sci.* **2009**, DOI doi:10.1016/j.pmatsci.2009.05.001.

COMMUNICATION